


Reconstruction of transverse-longitudinal vibrations in the organ of Corti complex via optical coherence tomography

Brian L. Frost,^{1,a)} Clark Elliott Strimbu,²  and Elizabeth S. Olson^{2,b)}

¹Department of Electrical Engineering, Columbia University, 500 West 120th Street, Mudd 1310, New York, New York 10027, USA

²Department of Otolaryngology Head and Neck Surgery, Vagelos College of Physicians and Surgeons, Columbia University, 630 West 168th Street, New York, New York 10032, USA

ABSTRACT:

Optical coherence tomography (OCT) is a common modality for measuring vibrations within the organ of Corti complex (OCC) *in vivo*. OCT's uniaxial nature leads to limitations that complicate the interpretation of data from cochlear mechanics experiments. The relationship between the optical axis (axis of motion measurement) and anatomically relevant axes in the cochlea varies across experiments, and generally is not known. This leads to characteristically different motion measurements taken from the same structure at different orientations. We present a method that can reconstruct two-dimensional (2-D) motion of intra-OCC structures in the cochlea's longitudinal-transverse plane. The method requires only a single, unmodified OCT system, and does not require any prior knowledge of precise structural locations or measurement angles. It uses the cochlea's traveling wave to register points between measurements taken at multiple viewing angles. We use this method to reconstruct 2-D motion at the outer hair cell/Deiters cell junction in the gerbil base, and show that reconstructed transverse motion resembles directly measured transverse motion, thus validating the method. The technique clarifies the interpretation of OCT measurements, enhancing their utility in probing the micromechanics of the cochlea. © 2023 Acoustical Society of America.

<https://doi.org/10.1121/10.0017345>

(Received 14 September 2022; revised 27 January 2023; accepted 3 February 2023; published online 23 February 2023)

[Editor: Hideko Heidi Nakajima]

Pages: 1347–1360

I. INTRODUCTION

Optical coherence tomography (OCT) is a powerful modality for the study of cochlear mechanics. It is capable of volumetric imaging and sub-nanometer-scale vibrometry at a depth into a sample^{1,2} allowing for the measurement of motion inside the organ of Corti complex (OCC) *in vivo*.^{3–9} OCT-derived findings have provided significant insight into OCC micromechanics, improving the understanding of and raising many questions about the mechanisms responsible for the impressive tuning and dynamic range of the sensitive cochlea.

OCT vibration measurements and images are built from one-dimensional (1-D) axial scans (A-Scans), generated via the Fourier transform of raw photodetector data. The magnitude of the A-Scan indicates the reflectivity at different depths into the sample. Images (referred to as brightness scans, or B-Scans) are built by taking a series of A-Scans along a line perpendicular to the optical axis (Fig. 1 shows a sample B-Scan of the OCC). Multiple parallel B-Scans can be taken to form a volume scan. A series of A-Scans at one location over a period of time is referred to as a motion scan (M-Scan). The phase of a single pixel in an M-Scan as a function of time is proportional to the sub-pixel displacement

in the direction of the beam axis of the structure at that pixel.² That is, an M-Scan allows us to measure the projection of the three-dimensional (3-D) motion of a structure onto the beam axis.

The nature of OCT leads to two important complications: (1) displacement measurements are 1-D projections of 3-D motions; (2) as OCT images are based on reflectivity, they are *label-free*—structures must be identified by known anatomy and experience. Each of these issues is further complicated by the fact that the optical axis is often decided due to the constraints of the preparation, and its relationship to the anatomy is often *a priori* unknown.

It is standard to define the *anatomical coordinates* of the cochlea as follows: the *longitudinal* axis points from base to apex along the spiral of the cochlea, the *radial* axis points from medial to lateral across the basilar membrane (BM) within a tonotopic cross section, and the *transverse* axis points from scala tympani to scala media normal to the BM [Fig. 1(B)]. As the measurement axis may have components in all of these anatomical directions, measured structures within a single A-Scan may lie in different longitudinal locations from one another.

In Frost *et al.*,¹⁰ we discuss a method that uses volume scans to determine the optical axes' relationships to these physiologically relevant axes. Using this method, one can account for the longitudinal distance between measured points in a single A-Scan—this was termed “skew correction,” and was studied by Cooper *et al.* The method

^{a)}Electronic mail: b.frost@columbia.edu

^{b)}Also at: Department of Biomedical Engineering, Columbia University, 351 Engineering Terrace, 1210 Amsterdam Avenue, New York, NY 10027 USA.

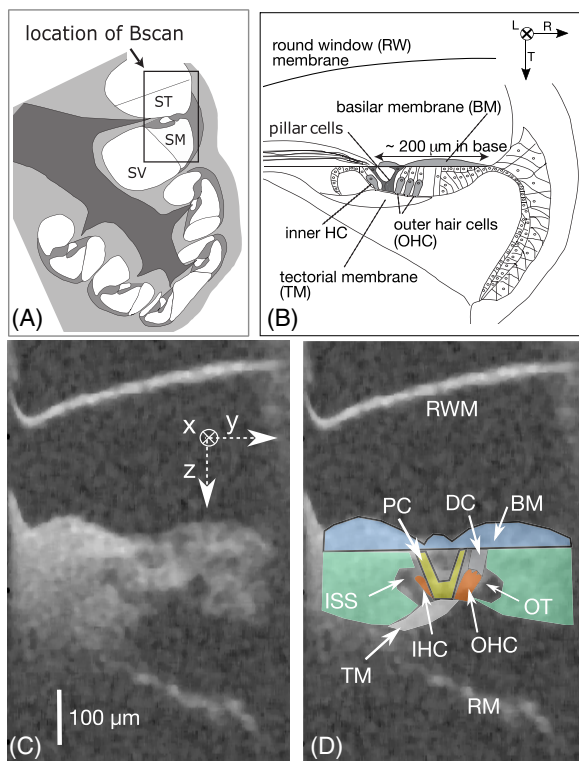


FIG. 1. (Color online) (A) Cartoon of the cochlea, with the location of the B-Scan marked. The B-Scans are taken through the round window membrane (RWM), so that scala tympani (ST) appears at the top of each image and scala media and vestibuli (SM, SV) appear towards the bottom. (B) Anatomical drawing of a tonotopic cross section of the cochlea with anatomical axes marked in the top right. The transverse direction points from scala tympani to scala media, the radial direction points from the spiral limbus to stria vascularis, and the longitudinal direction points from base to apex. (C) A B-Scan taken using our OCT system through the RWM in the hook region of the gerbil cochlea. The optical axis is predominantly transverse. (D) The B-Scan from panel (C) with overlaid labels of anatomical structures. RWM, round window membrane; BM, basilar membrane; PC, pillar cells; DC, Deiters cells; ISS, internal spiral sulcus; IHC, inner hair cells; OHC, outer hair cells; OT, outer tunnel; TM, tectorial membrane; RM, Reissner's membrane.

presented in Frost *et al.*¹⁰ also allows one to determine which components of motion are most represented in a measurement, offering more context to reported results. However, this is not sufficient to separate out the motion components themselves.

Cooper *et al.* showed the presence of intra-OCC longitudinal vibrations and argued that intra-OCC motion is elliptical. In elliptical motion, the phase of a structure's measured motion depends on viewing angle, leading to difficulty in interpretation of phase reported in 1-D measurements. As an example, purely transverse measurements in the gerbil base have shown different character than measurements taken at an angle relative to BM normal.^{11,12} While there are several differences that appear in data measured at different angles, in this work, we focus on the significant difference seen in outer hair cell/Deiters cell junction (OHC-DC) phase responses relative to BM.

Figure 2 shows three measurements of the phase responses in the OHC-DC region and at the BM in response

to a 70 dB stimulus. Measurements were corrected for skew, meaning that within each panel, data are presented from BM and OHC-DC within the same anatomical cross section. Figure 2(A) was taken at a nearly longitudinal angle near the 24 kHz place of the gerbil cochlea, Fig. 2(B) was taken at a nearly transverse angle in the hook region of the gerbil cochlea, and Fig. 2(C) was taken at a 64° angle with respect to the BM normal near the 26 kHz region in the gerbil base. The relative phase responses re BM are also shown for all three measurements. In the purely transverse case [Fig. 2(B)], OHC-DC lagged BM across frequency. On the other hand, when measured at a significant angle with respect to BM normal the response showed a *lead* of OHC-DC re BM across frequency.

These phase responses have distinct physical interpretations. These examples stress the impact of the measurement angle on the data acquired via OCT. The measurements in Fig. 2 differ in viewing angle and in best frequency location. With knowledge of the longitudinal and transverse components of motion at any given location, differences in response due to measurement angle can be better distinguished from differences due to location, or other variables, such as species and cochlear condition.

Recent efforts have been made to better understand intra-OCC motion at anatomically relevant angles, as these measurements aid in the understanding of cochlear micro-mechanics. One solution is to measure motion directly at an angle of interest. For example, Cho *et al.* measured at a transverse angle in the hook region of the gerbil base,¹¹ and He *et al.*¹² made purely transverse measurements of the reticular lamina in the gerbil base. However, such deliberate measurement angles are not available in all preparations and methods have been developed to reconstruct motion along physiologically relevant axes without directly measuring along these axes. Lee *et al.*⁸ used back-projection of measurements taken at two different angles to reconstruct radial-transverse motion in mouse, by carefully rotating the preparation to ensure the measured locations remained in the same optical cross section. Kim *et al.*¹³ used a three-beam OCT system in mouse to measure motion at the same location from three angles, and back-projected to resolve 3-D motion. These methods are challenging to implement in the gerbil base, where the anatomy and opacity of the bone significantly restrict the beam angle when viewing through the round window (RW). The latter method also requires more hardware and space than a single OCT device.

We have developed a method to reconstruct the longitudinal and transverse components of motion *in vivo* by OCT. As in the work of Lee *et al.*⁸ and Kim *et al.*,¹³ we reconstruct by back-projecting measurements taken at two angles. Our method performs registration using *physiology* rather than mechanical precision—it requires no *a priori* knowledge of either measurement angle, nor of the precise positions of the structures being measured. Instead, we use the traveling wave-induced phase on the BM and local linearization of the anatomical coordinates of the cochlea¹⁰ to register intra-OCC

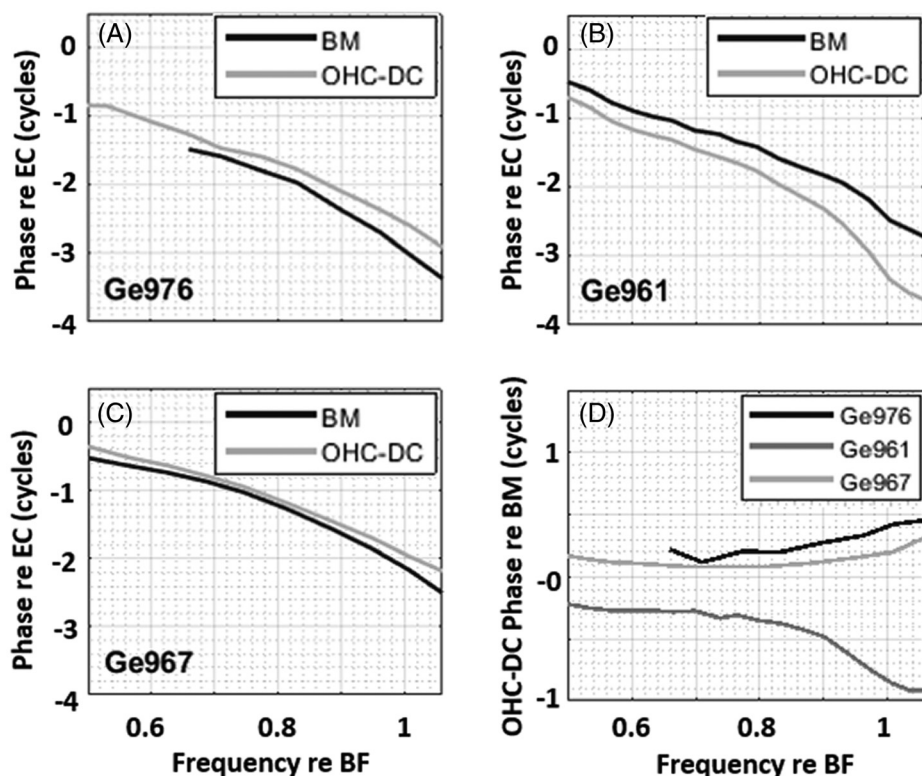


FIG. 2. Phase responses with respect to ear canal (EC) pressure at the BM and OHC-DC region in the gerbil base from three animals, in response to a 70 dB SPL (sound pressure level) Zwuis stimulus. (A) Displacement measurements at the 24 kHz location measured at an angle with a dominant longitudinal component. The viewing axis made an 80° angle with the BM normal. (B) Displacement measurements from the hook region (~50 kHz location) at an angle with a dominant transverse component. The viewing angle made an angle less than 10° with the BM normal. (C) Displacement measurements at the 26 kHz location at an angle with significant longitudinal and transverse components. The viewing angle made a 64° angle with the BM normal. (D) Relative phase of OHC-DC re BM, found by subtracting the two curves in each of panels (A–C). Measurements were corrected for skew, meaning that within each panel, data are presented from BM and OHC-DC within the same anatomical cross section.

positions between viewing angles. This allows the method to work in various species and preparations.

We present the method, an analysis of the accuracy of this method as a function of angular difference between two viewing angles, and *in vivo* experimental data taken through the RW in gerbil. We present longitudinal and transverse motion at the OHC-DC region, and see that the reconstructed transverse data match well with previous directly measured transverse OHC-DC motion in the gerbil base. In particular, transverse OHC-DC motion phase will be found to lag BM motion phase across frequency by ~0.3–0.4 cycles, save at high SPL where the two are observed to move in phase. This is in contrast with motion measured along a substantially longitudinal, apically directed axis, where a broadband phase lead of OHC-DC re BM is often seen.^{6,10,14}

II. METHODS

The method for reconstructing transverse–longitudinal motion in the OCC consists of three components: (1) “skew correction,” wherein BM and OHC-DC points are aligned within anatomical cross sections, (2) the registration of points on the BM between viewing angles, and (3) a mathematical reconstruction of transverse and longitudinal components of motion of the registered structures. To perform skew correction, we find the viewing axes’ angles relative to the BM normal, and determine how far apical OHC-DC points lie from BM points in the same A-Scan. To register BM points, we rely on the phase response of the BM. Under the assumption that BM motion is near-entirely transverse, BM phase responses at a single location will be

identical from any viewing angle. To perform the reconstruction, we apply a linear transformation to the motion data.

For this process, we assume that: (1) a local linear approximation of the longitudinal coordinate vector applies (i.e., that over a short distance, the cochlea can be considered non-coiled), (2) negligible radial component of motion is measured, (3) BM motion is near-entirely transverse, and (4) the imaging and condition of the cochlea remain stable during data collection. We provide a quantitative validation of these four assumptions at the end of the Results section.

A. Mathematics of reconstruction

The true motion of each structure is 3-D. However, our measurement angles were set to have a negligible radial component, so we will consider the “true motion” of a single point of interest as being a 2-D vector with only longitudinal and transverse components. (Radial motion will not be detected, and if present, it will not interfere with the reconstruction of longitudinal and transverse motion.) The longitudinal and transverse unit vectors are $\hat{\mathbf{l}}$ and $\hat{\mathbf{t}}$, respectively. The true displacement \mathbf{d} can be written as a two-vector with longitudinal and transverse components as

$$\mathbf{d} = d_l \hat{\mathbf{l}} + d_t \hat{\mathbf{t}}. \tag{1}$$

Importantly, $d \in \mathbb{C}^2$, meaning that each component has a magnitude and a phase.

The beam axis is a unit vector that can be written in anatomical coordinates, having a transverse and longitudinal component. Consider two such beam axes,

$$\hat{\mathbf{z}}_1 = l_1 \hat{\mathbf{l}} + t_1 \hat{\mathbf{t}}, \quad \hat{\mathbf{z}}_2 = l_2 \hat{\mathbf{l}} + t_2 \hat{\mathbf{t}}. \quad (2)$$

We take displacement measurements at a location of interest (registration described in Sec. II B) along both of these axes. These are 1-D displacements, δ_1 and δ_2 ; they are the projections of the true motion \mathbf{d} onto $\hat{\mathbf{z}}_1$ and $\hat{\mathbf{z}}_2$, respectively. Mathematically, this relationship is a dot product:

$$\delta_i = \hat{\mathbf{z}}_i^T \mathbf{d}, \quad i = 1, 2, \quad (3)$$

where each $\delta_i \in \mathbb{C}$ has a magnitude and a phase. We can also write this as a system of two equations in matrix form as

$$\begin{pmatrix} \delta_1 \\ \delta_2 \end{pmatrix} = \begin{pmatrix} l_1 & t_1 \\ l_2 & t_2 \end{pmatrix} \begin{pmatrix} d_l \\ d_t \end{pmatrix}, \quad (4)$$

or to solve for \mathbf{d} ,

$$\begin{pmatrix} d_l \\ d_t \end{pmatrix} = \begin{pmatrix} l_1 & t_1 \\ l_2 & t_2 \end{pmatrix}^{-1} \begin{pmatrix} \delta_1 \\ \delta_2 \end{pmatrix}. \quad (5)$$

The goal is to reconstruct the 2-D motion, i.e., to find \mathbf{d} . To do so, we need to measure δ_1 and δ_2 at the same location, and find anatomical coordinate representations of the measurement axes [i.e., the elements of the 2×2 matrix in Eq. (5)].

B. Experimental method

To perform the reconstruction according to Eq. (5), we (1) determine the measurement axes in anatomical coordinates

(l_i and t_i), and (2) register a point of interest between two orientations so that the same structure is measured at both angles. We present a method that performs both of these tasks without any *a priori* knowledge of precise structure locations or beam angles, using only a single OCT system. The process below is followed at both measurement angles $i = 1, 2$. Each step described below is graphically represented in a panel in Figs. 3 and 4.

1. Determining $\hat{\mathbf{l}}$

We begin with the OCT system viewing the OCC at the first orientation (measurement axis 1) and use the ThorImage software to produce a real-time volume scan at this angle. We find two points in the volume that lie on the anatomical structure of interest, and refer to their 3-D coordinates as \mathbf{p}_1 and \mathbf{p}_2 . These coordinates are read from the volume scan using ThorImage and are specified in optical coordinates, where $\hat{\mathbf{z}}_i$ is the optic axis (depth), and $\hat{\mathbf{x}}_i$ and $\hat{\mathbf{y}}_i$ are the scanning directions. In the example, shown in Fig. 3(A), \mathbf{p}_1 is chosen to lie at the OHC-DC junction in some cross section, and \mathbf{p}_2 to lie at the OHC-DC junction in a different cross section.

While the longitudinal and transverse directions are not constant in space—they change along with the spiral of the cochlea—one can approximate them as being stationary. This amounts to the local approximation of the BM as a plane, which is reasonable over a range of $\sim 200 \mu\text{m}$.¹⁰

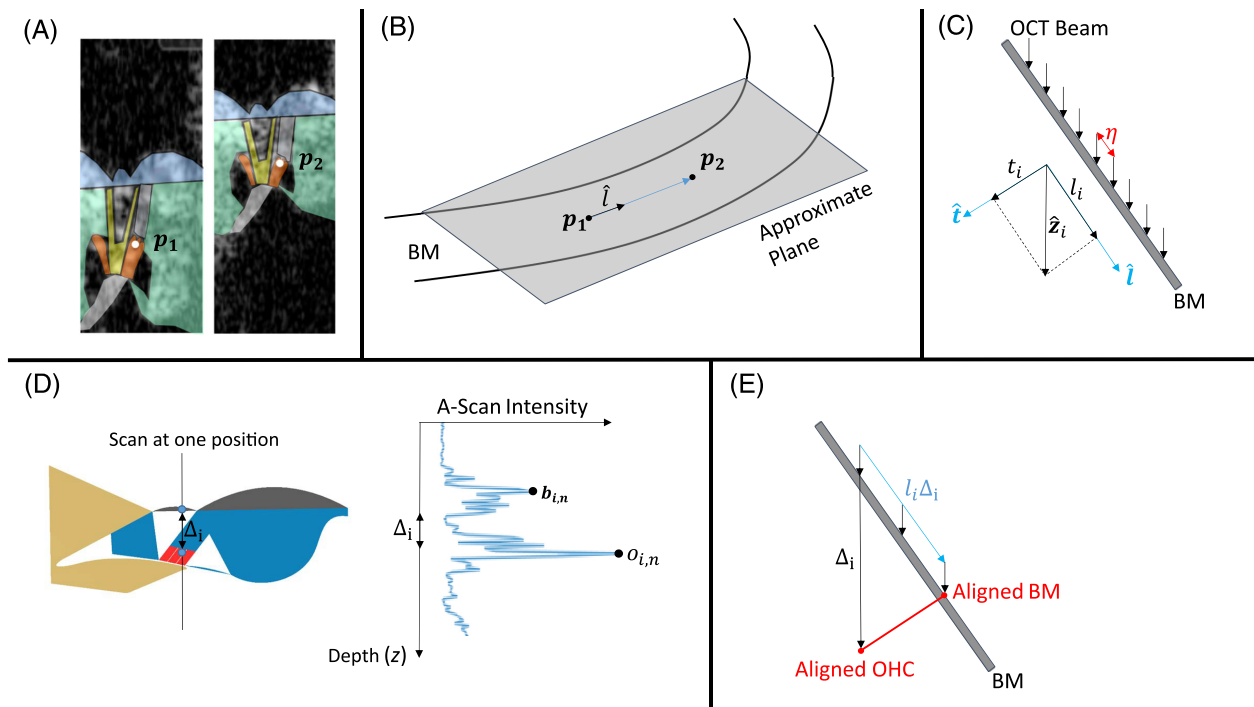


FIG. 3. (Color online) Graphical representation of the steps followed in the experimental method employed for 2-D reconstruction. (A) Labeled B-Scans from a single volume, with two points \mathbf{p}_1 and \mathbf{p}_2 at the same anatomical location (OHC-DC) marked in two different cross sections. (B) The BM approximated as a plane, in which the longitudinal direction connects any two points at the same anatomical structure between cross sections. (C) Cartoon of the BM with many measurements taken η apart longitudinally; anatomical axes with the measurement axis represented in longitudinal and transverse components. (D) Cartoon of OCC with points labeled at BM and OHC-DC, along with A-Scan with these same points labeled; Δ_i is the axial distance between OHC-DC and BM. (E) Cartoon of the BM with OHC-DC and BM in the same anatomical cross section but different A-Scans aligned by known longitudinal component of the measurement axis.

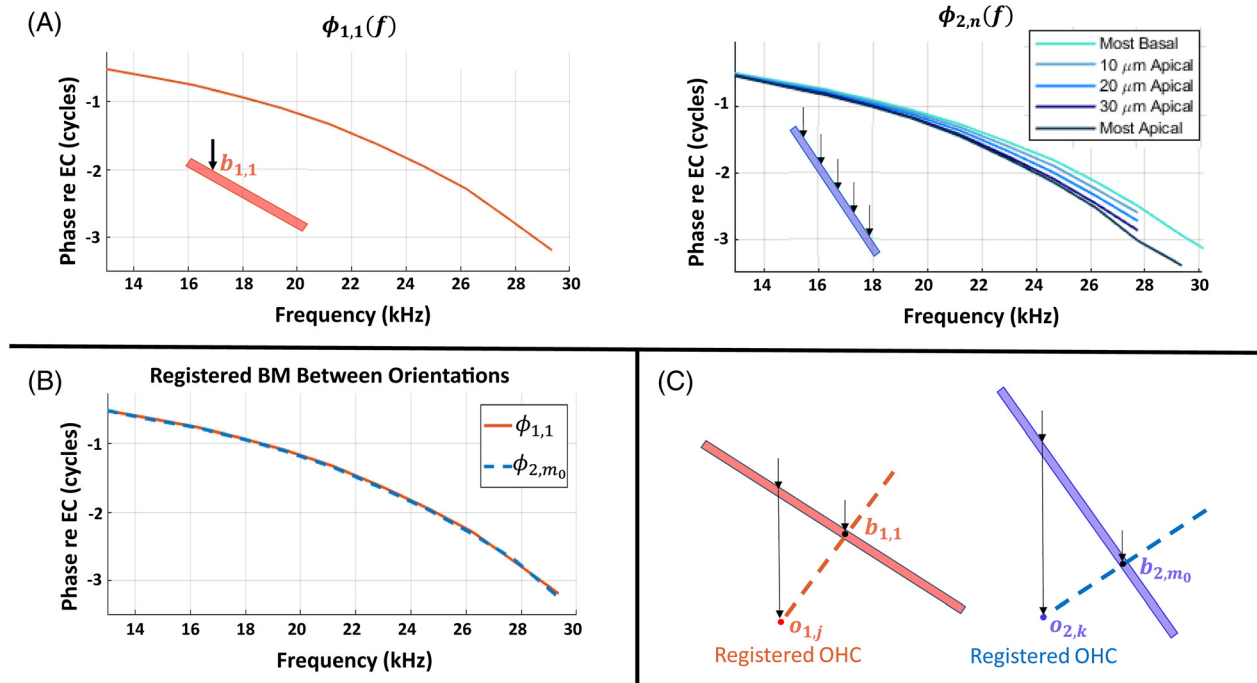


FIG. 4. (Color online) Graphical representation of the method by which cross sections and OHC-DC points are registered between orientation post-experiment. The pink and blue rectangles represent the short, approximately linear BM segments observed with the two orientations. (A) On the left, the first measured BM point’s phase response at 80 dB SPL, $\phi_{1,1}(f)$; on the right, a set of BM responses at 80 dB SPL taken $10\ \mu\text{m}$ apart longitudinally at the second orientation, $\phi_{2,n}(f)$ for $n = 1, 2, 3, 4, 5$. (B) $\phi_{1,1}(f)$ and the nearest phase response at orientation 2, ϕ_{2,m_0} . The two phase responses are nearly identical, showing that the BM points measured at $b_{1,1}$ and b_{2,m_0} are in the same anatomical cross section. (C) Cartoons of the BM at both orientations with registered BMs and cross sections shown in dotted lines. OHCs aligned to these BM points, $\mathbf{o}_{1,j}$ and $\mathbf{o}_{2,k}$, determined as in Fig. 3(E), are thereby also in the registered anatomical cross section. All four of these measured points lie in the same anatomical cross section, and the OHCs are thereby registered to one another as marked.

When approximated this way, the line segment connecting anatomical structures of the same type between cross sections is parallel to the longitudinal axis. The longitudinal unit vector is given in optical coordinates by

$$\hat{\mathbf{i}} = \frac{\mathbf{p}_2 - \mathbf{p}_1}{\|\mathbf{p}_2 - \mathbf{p}_1\|}. \quad (6)$$

This is displayed in Fig. 3(B). [As a clarifying aside, p_2 and p_1 are found for each of the two viewing angles to find the $\hat{\mathbf{i}}$ corresponding to each angle—the “2” and “1” in Eq. (6) do not indicate the two different viewing angles.]

2. Determining l_i and t_i

By the dot product, l_i , the component of the measurement axis $\hat{\mathbf{z}}_i$ in the longitudinal direction, is equal to the $\hat{\mathbf{z}}_i$ component of $\hat{\mathbf{i}}$ found in Eq. (6). Also, the measurement axis $\hat{\mathbf{z}}_i$ is a unit vector, so $l_i^2 + t_i^2 = 1$. This means that

$$t_i = \sqrt{1 - l_i^2}. \quad (7)$$

This is displayed in Fig. 3(C).

These steps find the elements of the matrix in Eq. (5) for the first measurement axis, $i = 1$. After reorienting the optics for the second angle, the matrix elements for the second measurement axis, $i = 2$, will be found in the same way.

3. Taking measurements along the longitudinal axis

To prepare to register points between orientations, before reorienting to the second angle, a set of N longitudinally spaced displacement measurements is taken at the first angle. The A-scan at the first longitudinal position includes \mathbf{p}_1 , a point in the OHC-DC region [Fig. 3(A)]. For any real a , $\mathbf{p}_1 + a\hat{\mathbf{i}}$ is also in the OHC-DC region. We choose a number of points N and a spacing η , and take measurements at points

$$\mathbf{p}_n = \mathbf{p}_1 + (n - 1)\eta\hat{\mathbf{i}}, \quad n = 1, \dots, N. \quad (8)$$

This gives N measurements of the structure evenly spaced longitudinally, as displayed in Fig. 3(C).

4. Relating BM and OHC-DC within each A-Scan

In each measurement line (A-scan), we always measure BM motion. We refer to BM and OHC points measured in A-Scan n at orientation i as $\mathbf{b}_{i,n}$ and $\mathbf{o}_{i,n}$, respectively. Because the beam axis has longitudinal and transverse components (i.e., $\hat{\mathbf{z}}_i \neq \hat{\mathbf{i}}$), the OHC-DC and BM points measured in each A-Scan are not in the same longitudinal cross section. Suppose that on the $\hat{\mathbf{z}}_i$ axis in a single A-Scan, $\mathbf{b}_{i,n}$ and $\mathbf{o}_{i,n}$ are $\Delta_i = (\mathbf{o}_{i,n} - \mathbf{b}_{i,n}) \cdot \hat{\mathbf{z}}_i$ apart. The longitudinal distance between the BM and OHC points observed in a single A-Scan is thereby $l_i\Delta_i$ [Figs. 3(D) and 3(E)]. We assume that,

for each orientation angle, this value is independent of the cross section n .

5. Aligning BM and OHC at each orientation

Consider the first OHC-DC measurement at $\mathbf{o}_{i,1}$. As we found above, it is in the same anatomical cross section as a point on the BM at $\mathbf{b}_{i,1} + l_i \Delta_i \hat{\mathbf{l}}$. We have taken many measurements of BM along the longitudinal axis, so if the space between measurements η is small, there exists an integer m such that $l_i \Delta_i \approx m\eta$. That is, $\mathbf{o}_{i,1}$ is approximately in the same anatomical cross section as $\mathbf{b}_{i,m+1}$ for this m . This alignment process is shown in Fig. 3(E). We repeat this process for all measured OHC-DC points to form a list of *aligned* OHC-DC/BM pairs (i.e., OHC-DC and BM in the same anatomical cross section) at each orientation. Using this list, we reformulate the problem of registering OHC-DC points as one of registering BM points—the OHC-DC points aligned to these BM points will also be registered.

6. Registering BM points between orientations

The remaining steps are performed after the experiment, using collected data. The steps are graphically represented in Fig. 4. To register BM points between orientations, we use the traveling wave. We assume that the BM moves entirely transversely. As a result, the phase response of BM motion will be the same at every viewing angle. To register points on the BM between orientations, we compare the phase response at $\mathbf{b}_{1,n}$ to $\mathbf{b}_{2,m}$ for $n, m = 1, 2, \dots, N$, and find the values for which the phase responses are most similar by minimum L_2 distance. We start by comparing the phase response at $\mathbf{b}_{1,1}$ to $\mathbf{b}_{2,m}$ for $m = 1, \dots, N$. We call these responses $\phi_{1,1}(f)$ and $\phi_{2,m}(f)$, respectively, where f is frequency. We find

$$m_0 = \underset{m}{\operatorname{argmin}} \|\phi_{1,1}(f) - \phi_{2,m}(f)\|, \tag{9}$$

and consider $\mathbf{b}_{1,1}$ and \mathbf{b}_{2,m_0} to be registered (the argmin gives the value of m that minimizes the expression). Because BM positions measured are spaced longitudinally by η at both orientations, $\mathbf{b}_{1,2}$ and \mathbf{b}_{2,m_0+1} are also registered, and so on. This yields registered BM points across some longitudinal range of the BM. Figure 4(A) illustrates the process, showing the phase response at point 1, orientation 1, and the phase responses across longitudinal position at orientation 2. We compare the phase response $\phi_{1,1}(f)$ to all of the phase responses at orientation 2 and find the best match, $\phi_{2,m_0}(f)$. This match is shown in Fig. 4(B), wherein the phase responses are nearly identical. This means that the cross sections containing these two BM points are identical.

7. Registering OHC-DC points between orientations

To register OHC-DC points between orientations, we synthesize information from the last two steps. Say BM points $\mathbf{b}_{1,n}$ and $\mathbf{b}_{2,m}$ are registered. Recall that we *aligned* these BM points to OHC-DC points in the same anatomical

cross section. If $\mathbf{b}_{1,n}$ is aligned to OHC-DC point $\mathbf{o}_{1,j}$ and $\mathbf{b}_{2,m}$ is aligned to $\mathbf{o}_{2,k}$, then *all four* of these measured points are in the same anatomical cross section. This means that these two OHC-DC points are registered, and we can do this for all registered BM points with aligned OHC points. This is graphically represented for a single position in Fig. 4(C), and across the entire measurement range in Fig. 5.

Having found the longitudinal and transverse components of the two measurement axes, and registered OHC-DC points, the mathematical reconstruction as developed in Sec. II A can be performed. We used the example of the OHC-DC structure, but this can be done for any structure in the OCC.

C. Error dependence on angular difference

The presentation above is in an ideal environment, wherein the reconstruction can be performed from any two measurements at distinct angles. Mathematically, the error associated with the angular difference arises from the matrix in Eq. (5). This matrix must be invertible, which requires that its rows are not collinear. The rows of this matrix are the measurement axes, $\hat{\mathbf{z}}_1$ and $\hat{\mathbf{z}}_2$, which are not collinear by design. The invertibility of the matrix is thereby guaranteed. However, it is intuitively clear that reconstructions could not be reliably made from two measurements taken, say, only 1° apart. This lies in the fact that the matrix has a multiplicative impact on the noise in measurements δ_1 and δ_2 . As a rule of thumb, if σ_{max} and σ_{min} are the maximum and minimum singular values of a matrix, then matrix multiplication increases the noise level by a factor of the *condition number*:

$$\kappa = \frac{|\sigma_{max}|}{|\sigma_{min}|}. \tag{10}$$

A matrix and its inverse have the same condition number. The formulae for the singular values of a 2×2 matrix (using the element names of the relevant matrix) are

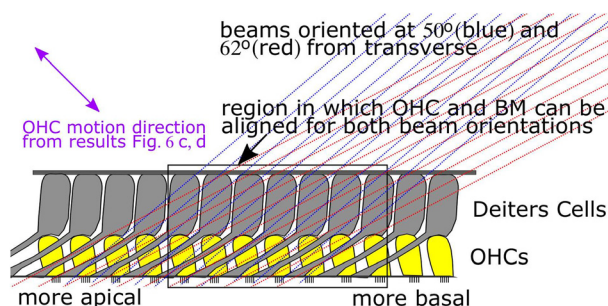


FIG. 5. (Color online) Cartoon of a longitudinal-transverse cross section of the OCC containing the Deiters cells and OHCs. Measurement axes at two orientations that are achievable through the gerbil RW are shown. Measured OHC and BM positions along one measurement axis will lie at different longitudinal locations. Eleven measurements at each angle are taken $10 \mu\text{m}$ apart longitudinally. The boxed region shows positions at which we can align measured BM positions with measured OHC-DC positions—this corresponds to about six distinct OHC-DC positions being registered. The arrow in the top-left shows the direction of motion in which the OHC-DC region was found to move in the reconstruction shown in Fig. 6.

$$\sigma_{max} = \sqrt{\frac{s_1 + s_2}{2}}, \tag{11}$$

$$\sigma_{min} = \sqrt{\frac{s_1 - s_2}{2}}, \tag{12}$$

where

$$s_1 = l_1^2 + t_1^2 + l_2^2 + t_2^2, \tag{13}$$

$$s_2 = \sqrt{(l_1^2 + t_1^2 - l_2^2 - t_2^2) + 4(l_1 l_2 + t_1 t_2)^2}. \tag{14}$$

The measurement axes are unit vectors, so $l_i^2 + t_i^2 = 1$ for $i=1, 2$. That gives $s_1 = 2$ and $s_2 = 2(l_1 l_2 + t_1 t_2)$. Defining $\nu = l_1 l_2 + t_1 t_2$, we simplify the condition number formula to

$$\kappa = \sqrt{\frac{1 + \nu}{1 - \nu}}, \tag{15}$$

a monotonically increasing function of ν .

Note that $\nu = \hat{\mathbf{z}}_1 \cdot \hat{\mathbf{z}}_2$, which may offer a bit of intuition—the dot product increases as the angular difference approaches 0, yielding an increase in condition number. To be more mathematically precise,

$$\nu = \|\hat{\mathbf{z}}_1\| \|\hat{\mathbf{z}}_2\| \cos \theta = \cos \theta, \tag{16}$$

where θ is the angular difference between the two vectors and we have used the fact that the measurement axes are unit vectors. Trigonometric identities allow the condition number to be written succinctly as a function of the angular difference between the two measurement axes:

$$\kappa = \sqrt{\frac{1 + \cos \theta}{1 - \cos \theta}} \tag{17}$$

$$= \sqrt{\frac{1}{\tan^2 \frac{\theta}{2}}} \tag{18}$$

$$= \frac{1}{\left| \tan \frac{\theta}{2} \right|}, \quad -90^\circ \leq \theta \leq 90^\circ. \tag{19}$$

The condition number goes to infinity when the angular difference approaches 0, and approaches a minimum at 1 as the angular difference approaches 90°. While 90° would be optimal, the maximum achievable angular difference is restricted by the experimental preparation. For example, in measurements taken through the gerbil round window, 15° is often the largest achievable angular difference. The noise floor of our displacement measurements is approximately 0.1 nm. For a vector of two independent measurements δ_1 and δ_2 , the noise floor would thereby be about $\sqrt{0.1^2 + 0.1^2} \approx 0.14$ nm. The noise increase induced by reconstruction using measurements taken 15° apart [a κ value of 7.6 according to Eq. (19)] would yield a noise floor of ~ 1 nm.

D. Basic stimulus protocol

The present work describes analytical reconstruction following data collection. A detailed description of the *in vivo* experimental methods, including the animal surgery and OCT vibrometry, can be found in Strimbu *et al.*⁶ In brief, motion measurements were made with a Thorlabs Telesto 3 OCT system with a central wavelength of 1300 nm equipped with an LSM03 5× objective lens. Acoustic stimuli were 1 s, 15 tone Zwis stimuli that spanned a frequency range from 12–36 kHz (Ge967), 10–30 kHz (Ge976), and 20–50 kHz (Ge961). At the start of each experiment, vibrations were measured in response to a Zwis complex at a single longitudinal location close to the intersection of the arcuate and pectinate zones near the OHCs, and the estimated best frequency was used to select an appropriate frequency range for subsequent measurements. Stimulus delivery and data acquisition used a Tucker Davis Technologies system whose clock signal was used to trigger the OCT as previously described. Ear canal pressures were monitored with a Sokolich ultrasonic probe microphone. In addition to the Zwis stimuli used for motion measurements, two-tone stimuli with frequencies f_1 and f_2 were used to measure distortion product otoacoustic emissions (DPOAEs) as a monitor of cochlear condition. Here, f_2 varied from 2–48 kHz and the two frequencies were presented at 50 and 70 dB SPL with a fixed ratio $f_2/f_1 = 1.2$. DPOAEs were measured at the start of the motion measurements following the initial surgery and at selected times throughout each experiment, and were typically stable.

III. RESULTS

We begin with an example of the method applied in a single *in vivo* gerbil preparation, wherein measurements were taken through the RW. Using values of $l_1, t_1, l_2,$ and t_2 found using the methods described in Figs. 3(A)–(C), the measurement axes in this experiment made 64° and 50° angles with the BM normal at orientations 1 and 2, respectively. The angular difference, 14°, yielded a measurement matrix with condition number $\kappa \approx 8$. This is the factor by which the noise level is increased as a result of reconstruction. We show results at SPLs as low as 40 dB, but focus on 70 dB and 80 dB SPL responses because the reconstructed signal was significant at these SPLs through a relatively wide frequency range.

A. Example of a single reconstruction

Figure 6 shows a reconstruction using responses to the 80 dB SPL stimulus. In this example, from the first angle, we consider data from the OHC-DC region measured at the fourth measurement location: $\mathbf{o}_{1,4}$. Skew correction is performed to align BM and OHC within the same anatomical cross section: Using the value of l_1 , the longitudinal distance between BM and OHC-DC locations along measurement axis 1 was about 40 μm [Figs. 3(C)–(E)]. The longitudinal spacing [η in Fig. 3(C)] was 10 μm , thus $\mathbf{o}_{1,4}$ is in the same anatomical cross section as $\mathbf{b}_{1,8}$.

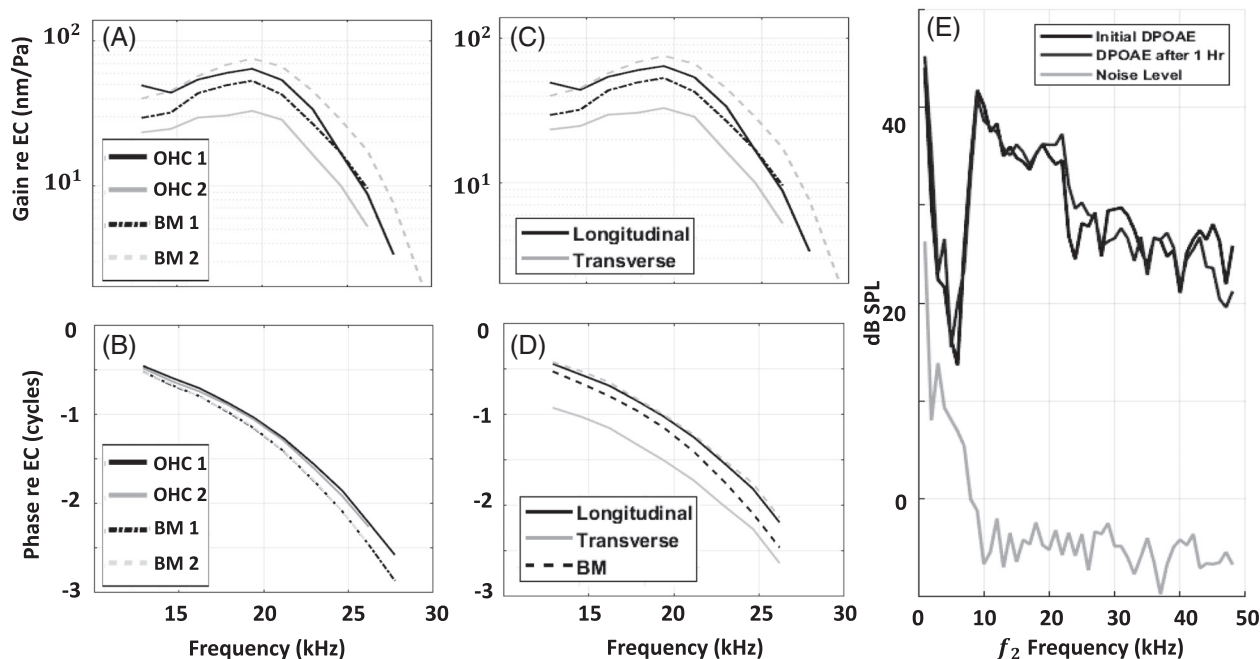


FIG. 6. An example of responses and corresponding reconstruction from Gerbil 967 at registered OHC-DC positions performed using responses to an 80 dB 15-frequency, 1 s Zwuis stimulus. (A) and (B) Magnitude and phase responses at aligned OHC-DC positions taken at two orientations—viewing angles 1 and 2 make 64° and 50° angles with the BM normal, respectively. BM responses in the registered cross section measured at both orientations are also shown. Note that the BM phase responses are nearly indistinguishable between orientations, indicating that the cross section is truly registered. Similarly, the BM magnitudes are parallel (offset vertically), and differ by a geometric factor determined by the ratio of the measurement angles' cosines. (C) and (D) Reconstructed longitudinal and transverse magnitude and phase responses at the OHC-DC, generated by application of Eq. (5) to the data in panels (A) and (B). For reference, we also show the BM phase response as a dashed black line, and the dashed gray line shows the reconstructed transverse phase shifted vertically by 0.5 cycles. (E) DPOAE magnitudes in response to 70 dB SPL two-tone stimuli measured 20 min prior to the displacement measurements at each orientation. These two DPOAE measurements were taken 1 h apart.

The registration of BM points between orientations used least squares matching of $\mathbf{b}_{1,1}$ and $\mathbf{b}_{2,m}$ phase responses for $m = 1, \dots, 11$, as shown in Fig. 4. The data in Fig. 4 are from the experiment we are using in this example, and we found $\mathbf{b}_{1,1}$ to be registered to $\mathbf{b}_{2,2}$. This means that $\mathbf{b}_{1,8}$ is registered to $\mathbf{b}_{2,9}$. Finally, using the value of l_2 , the longitudinal distance between BM and OHC-DC locations was about $30 \mu\text{m}$, and thus $\mathbf{o}_{2,6}$ is in the same anatomical cross section as $\mathbf{b}_{2,9}$.

Now, the registration is complete: $\mathbf{b}_{1,8}$, $\mathbf{o}_{1,4}$, $\mathbf{b}_{2,9}$ and $\mathbf{o}_{2,6}$ are all in the same anatomical cross section. Figures 6(A) and 6(B) show the displacement frequency responses measured at these OHC-DC points at the two angles. These complex data would correspond to δ_1 , δ_2 in Eqs. (4) and (5). The displacement phases at the two registered BM locations are also shown and are nearly identical, as they must be if the registration method is reasonable. Moreover, BM amplitudes should be parallel (offset from each other vertically) and differ by a geometric factor— $\cos \theta_2 / \cos \theta_1 \approx 1.47$. We can see that the BM responses are quite nearly parallel, and we compute that they differ in size by a factor of, on average, 1.43.

Finally, we perform the reconstruction. The components l_1 , t_1 , l_2 , and t_2 form the reconstruction matrix [Eq. (5)], which we apply to the directly measured displacements, δ_1 and δ_2 . The reconstructed longitudinal and transverse OHC-DC frequency responses are shown in Figs. 6(C) and 6(D).

We performed this mathematical reconstruction at six registered OHC-DC points, as in the cartoon in Fig. 5. An example of reconstructed transverse and longitudinal gain

responses in the OHC-DC region are shown in Fig. 7. Longitudinal and transverse gain and phase responses in response to 70 and 80 dB SPL Zwuis stimuli at two positions, alongside BM data from the same cross section, are shown in Fig. 8.

The reconstructed transverse and longitudinal motion are out of phase by approximately half a cycle across most of the frequency range. This is made clear with the light gray dashed line in Fig. 6(D), which shows transverse phase shifted upwards by half of a cycle. This indicates non-elliptical (i.e., straight line) motion along an axis that lies between the positive longitudinal and negative transverse directions. This direction of motion is indicated in the purple arrow in Fig. 5. The amplitude of the measured motion was significantly larger at orientation one (the more longitudinal measurement angle) than at orientation two. This δ_1 and δ_2 combination could result from the longitudinal component being much larger than the transverse component. However, the angular difference of 14° is too small to account for the size of the loss in amplitude at the second orientation. A more plausible explanation for the smaller amplitude at the second orientation is that the second angle of observation is more perpendicular to the direction of overall motion. This reasoning also explains why the reconstructed transverse and longitudinal responses are larger than the amplitude of the motion measured at either orientation. This sort of “cancellation” effect will be strongest when the motion is nearly linear (not elliptical) because elliptical motion will

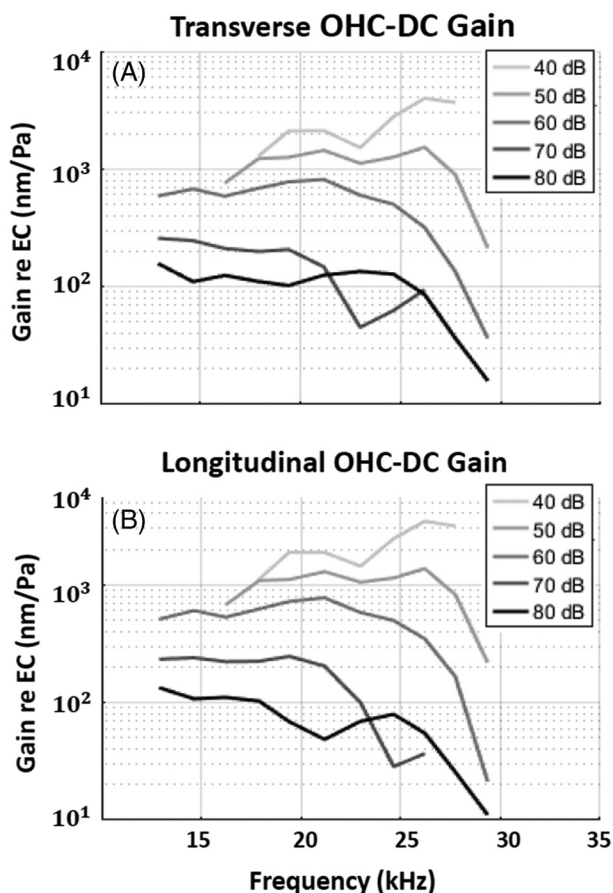


FIG. 7. Transverse and longitudinal gain responses re EC from Gerbil 967, reconstructed from OHC-DC motion measured in the gerbil base at two angles in response to Zwuis stimuli at various SPLs. (A) and (B) Transverse and longitudinal tuning curves reconstructed from OHC-DC at the location at which SNR was highest. Presented displacements were at least 1 standard deviation above the noise level and the displacements measured in response to 70 and 80 dB stimuli were at least 2.5 standard deviations above the noise level. Note the presence of broadband nonlinearity.

never be perpendicular to the observation direction. Finally, the observation that the OHC-DC phase responses measured at the two orientations [as in Fig. 6(B)] are nearly equal is consistent with nearly linear motion.

B. Validation of assumptions

The method operates under the assumptions that (1) the longitudinal axis of the cochlea can be approximated as a line in the region of interest, (2) the radial component of motion measurement is negligible, i.e., the A-scan axis is perpendicular to the radial axis, (3) the motion of the BM is near-entirely transverse, and (4) the imaging and condition of the cochlea is stable over the course of the experiment.

1. The linear approximation of the longitudinal coordinate vector

To validate the first assumption, we considered an OCT volume scan of the gerbil cochlea base, taken near the 25 kHz location. We selected 10 points (in optical XYZ coordinates) along a 440 μm longitudinal span of the cochlea,

lying at the point at which the spiral lamina meets the BM. These 10 points lie along the curve defined by the true, spatially varying, longitudinal direction. We measured the nearness of the points to a line by finding the point-set's autocorrelation matrix and squaring it point-wise. This symmetric matrix comprises three correlation coefficients that quantify the nearness of the point-set to a line within each coordinate plane, with a value of 1 indicating a perfect fit to a line. The line of best fit was also found for five-point sets along half of the span. Figure 9 shows the point-set along with the line of best fit projected onto each coordinate plane. It is apparent that the fit is reasonable for the 10-point segment, and the five-point (220 μm) segment is very close to a line. Recalling that the data were taken along less than half this span—100 μm , longitudinally—the linear assumption is reasonable.

2. The radial component of measurement

In general, the measurement (optical) axis \hat{z} will contain longitudinal, radial, and transverse components. In the procedure described in this study, we eliminate the radial component by orienting the preparation such that the optical axis is perpendicular to the plane of the BM. To check the accuracy of this, we used the orientation program described in Frost *et al.*¹⁰ to determine the coefficients of \hat{z} in anatomical coordinates— z_l , z_r and z_t —at each of the measurement angles. These correspond to the weights with which each component of motion contributes to the total measured motion. Near the 26 kHz place, we can consistently reduce the radial weight z_r to be at least an order of magnitude less than the longitudinal and transverse weights. As an example, at orientation 1 in the experiment of Fig. 8, the measurement axis is given by $\hat{z} = (z_l \ z_r \ z_t) \approx (0.90 \ 0.02 \ 0.43)$. The radial component contributes ~ 20 times less than transverse motion, and ~ 40 times less than longitudinal motion to the total measured motion at this angle. Our assumption of negligible radial motion in the measurement is valid as long as the radial motion at the structure of interest is not an order of magnitude larger than the other components of motion.

3. Basilar membrane moves mostly transversely

It has been argued that BM motion is likely to be totally transverse. The anatomy of the BM does not facilitate motion in the radial or longitudinal direction. The BM comprises densely packed radial fibers, clamped at both radial edges, forming a contiguous unit with the spiral lamina and spiral ligament.¹⁵ Moreover, as longitudinal shearing fluid motions are expected to be antisymmetric and similar in size, there is no expected net shear on the BM to drive longitudinal motion.^{16,17}

4. Acquisition time and yield

The measurements in the example experiment (Gerbil 967) were taken over about 2 h. Each 1 s Zwuis stimulus takes 10 s to acquire, process, and transfer to a hard drive

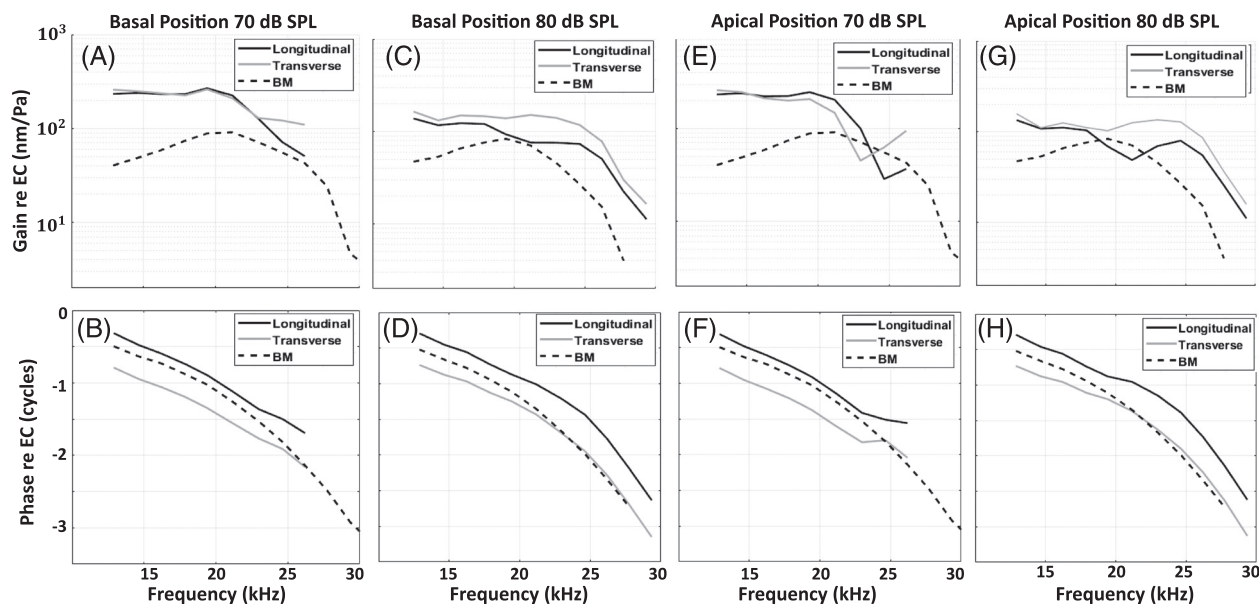


FIG. 8. Transverse and longitudinal gain and phase responses reconstructed at the OHC-DC in response to Zwuis stimuli at 70 and 80 dB SPL at two distinct longitudinal locations. The measurement positions are spaced apart by $60 \mu\text{m}$ longitudinally. Light gray curves are reconstructed transverse OHC-DC responses, dark gray curves are reconstructed longitudinal OHC-DC responses, and black dashed curves are BM responses in this same cross section (Gerbil 967).

(data transfer from random access memory to the hard drive is the most time-consuming step). Taking measurements at 5 SPLs at 11 locations at two angles would take 1100 s—less than 20 min. Additional time was spent ensuring the stability of the imaging and measuring DPOAEs. Time was also spent rotating the preparation so that a substantial angular difference could be achieved between the two measurements while still viewing the same frequency location, and with the radial axis perpendicular in the B-scan view.

It is critical to ensure that the results are not impacted by instability of either imaging or the condition of the cochlea.

The most common cause of image instability is the accumulation of fluid on the RWM, which has a lensing effect that impacts the imaging and measurement angle. Fluid accumulation was alleviated by placing an absorbant cotton wick near the RW opening. In the experiment from which the presented data were acquired, after motion was measured at each longitudinal location, we checked that the image had not shifted more than $8 \mu\text{m}$ (the lateral resolution of our system) from its original state in any of the three optical directions.

The condition of the cochlea was assessed by periodically measuring DPOAEs. Over the course of the

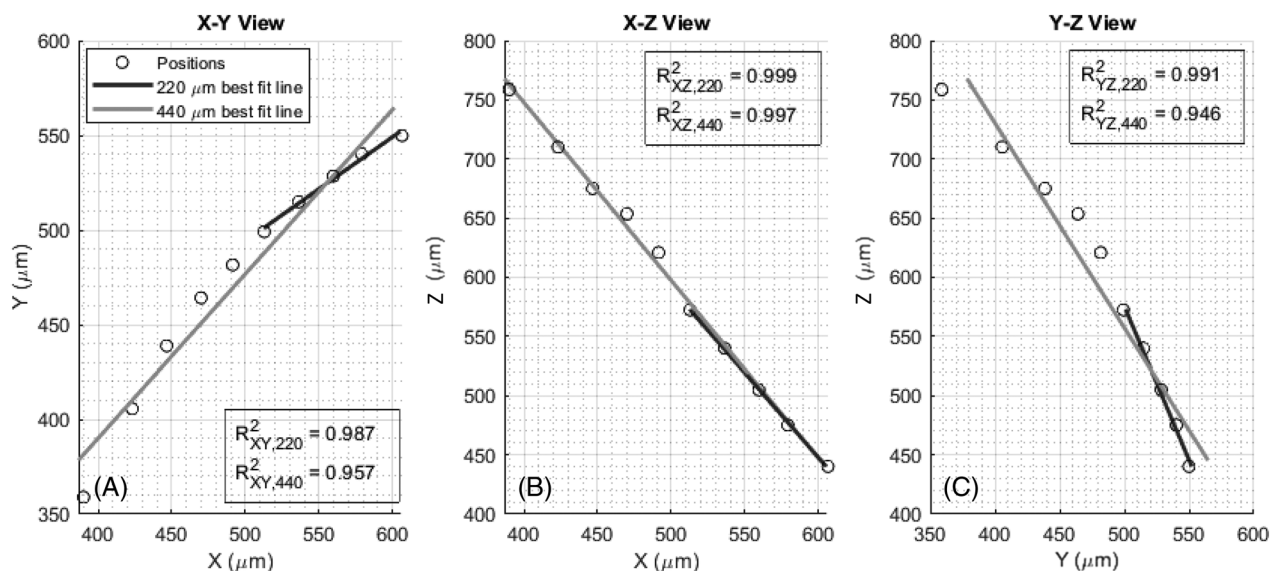


FIG. 9. Points along the cochlear spiral chosen at the junction between BM and spiral lamina. Each panel shows the selected points in open black circles, along with the lines of best fit over both a $220 \mu\text{m}$ and $440 \mu\text{m}$ longitudinal span of the cochlea, projected onto the three optical planes. These are (A) the X-Y plane; (B) the X-Z plane; (C) the Y-Z plane. (The registration method used a $100 \mu\text{m}$ longitudinal span, so linearity even over the $220 \mu\text{m}$ range is beyond what is required.) The corresponding correlation coefficients are also shown. The points trace out the true spatially varying longitudinal direction, while the lines of best fit represent the linear approximation.

experiment, we did not see significant degradation in these responses. An example is shown in Fig. 6(E).

IV. DISCUSSION

We begin the discussion by comparing the reconstructed transverse and longitudinal displacements to displacements that were directly measured with those orientations. We follow with physiological interpretations, motivating future applications of the reconstruction method.

A. Features of the data and comparison to previous measurements

In the OHC-DC region gain plots in Fig. 7, transverse and longitudinal components of OHC-DC motion exhibit broadband nonlinearity, which is characteristic of past OHC measurements made using Zwuis stimuli.^{5,6,18} In Fig. 8, OHC-DC motion in the longitudinal and transverse direction is tuned to approximately the same frequency as the BM, but shows more frequency structure than BM motion. Transverse and longitudinal components of motion have similar magnitude at 70 dB SPL (the lines nearly overlies) but transverse motion is larger than longitudinal at 80 dB SPL. Although the two locations in Fig. 8 were spaced longitudinally by 60 μm, the amplitude appears to be tuned to the same best frequency (BF). This is not surprising; the place-frequency map in the gerbil base has a slope of about 1 decade/5.4 mm,¹⁹ and along 60 μm, these mildly peaked responses are not expected to change discernibly. However,

the tonotopic change can be seen in the phase responses in Fig. 4(A), which is the basis for the registration.

In the phase response curves in Fig. 8, at 70 dB SPL, the transverse component of OHC-DC motion lags BM across frequency by ~0.3–0.4 cycles. At 80 dB SPL and near the BF, the OHC-DC transverse component and BM move approximately in phase. The longitudinal component is approximately half a cycle out of phase from transverse displacement across much of the tested frequency range. This means that base-to-apex motion is approximately in phase with scala media-to-scala tympani motion.

To explore the reliability of the reconstructed results, we compare to previously measured displacement phase responses taken at dominantly longitudinal or dominantly transverse angles. The responses shown in Figs. 10(A) and 10(C) (measurements at 70 and 80 dB SPL, respectively) were measured at a dominantly longitudinal angle, with the measurement axis making an 80° angle with the BM normal. For comparison, Figs. 10(B) and 10(D) show reconstructed longitudinal phase responses. Figures 10(E) and 10(G) show phase responses measured at a largely transverse measurement angle, while Figs. 10(F) and 10(H) show reconstructed transverse phase responses.

Focusing first on the phase responses in longitudinal motion, a broadband lead of OHC-DC re BM is present in the directly measured and reconstructed responses. In the 80 dB SPL case, the lead is smaller at low frequencies than at frequencies near the BF. This increasing-with-frequency lead is more pronounced in the reconstructed responses.

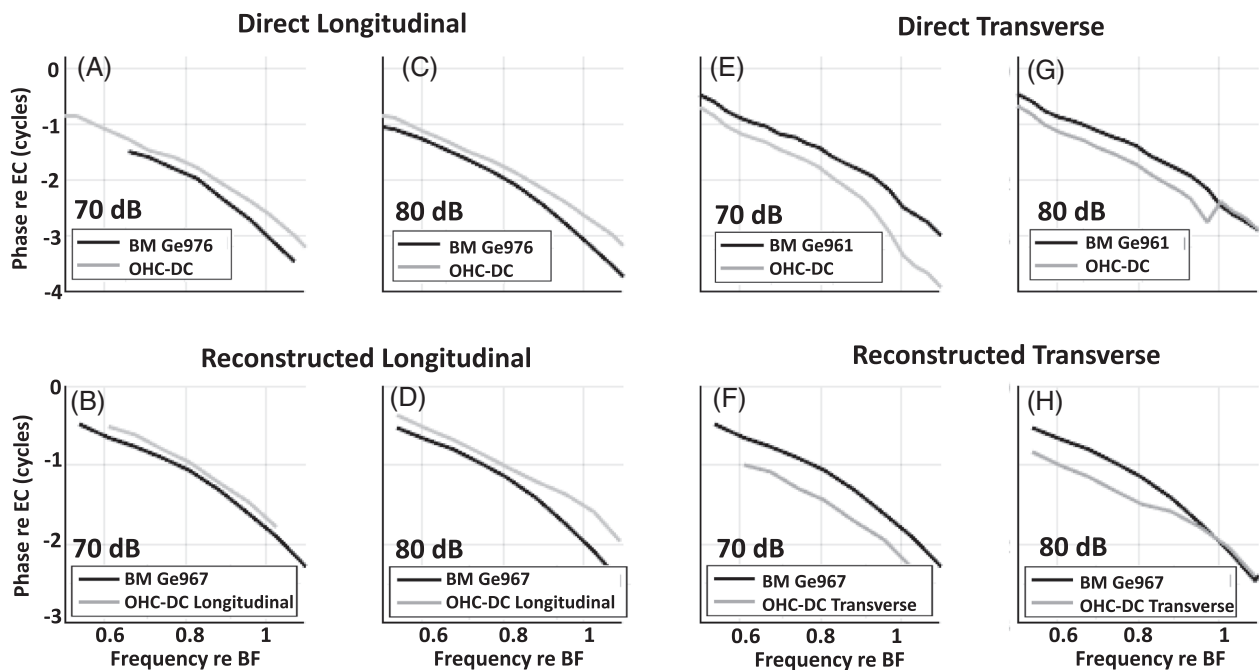


FIG. 10. OHC-DC (light gray) and BM (black) phase responses from experiments in which a primarily longitudinal or transverse angle was set, compared to the reconstructed longitudinal and transverse phase responses. (A) and (C) Phase responses measured at a nearly longitudinal angle $\theta \approx 80^\circ$ in the gerbil base (BF ≈ 24 kHz) using Zwuis stimuli at 70 and 80 dB SPL, respectively. (B) and (D) longitudinal OHC-DC phase responses reconstructed using the method at a single longitudinal location (BF ≈ 26 kHz). (E) and (G) Phase responses measured at a nearly transverse angle $\theta < 10^\circ$ in the hook region (BF ≈ 50 kHz) using Zwuis stimuli at 70 and 80 dB SPL, respectively. (F) and (H) Transverse OHC-DC and BM phase responses reconstructed using the method at a single longitudinal location (BF ≈ 26 kHz). Note that both the directly measured and reconstructed transverse OHC-DC phase lags BM phase across frequency, but becomes in phase at higher SPLs near the BF.

As for transverse motion, a broadband lag of OHC-DC re BM is present in the directly measured and reconstructed responses. At 70 dB SPL, the reconstructed OHC-DC phase lags BM by about 0.2–0.3 cycles. In the directly measured phase response, this lag is smaller at low frequencies and larger at high frequencies, with a value of 0.2–0.3 cycles near 0.8 BF. At 80 dB SPL, the reconstructed and directly measured OHC-DC phase undergo a large “lift” at higher frequencies, so that OHC-DC and BM phase are nearly equal above about 0.9 BF. In the reconstruction, this transition is smooth, whereas it is sudden in the directly measured case.

While qualitative features of the data are similar in the reconstructed and directly measured displacements, there are quantitative differences in the magnitudes of phase lags/leads. For the transverse motion comparison in Figs. 10(E) and 10(H), the BF of the locations in directly measured and reconstructed responses was not the same: in Ge961 [Figs. 10(E) and 10(G)], the BF was 50 kHz, and in Ge967 [Figs. 10(F) and 10(H)], BF was 26 kHz. This substantial BF location difference might introduce quantitative variations. The condition of the preparation or basic cochlear variability may also introduce differences between experiments. One of the objectives of this study is to develop methodology to isolate BF location and preparation-based differences from differences caused by the observation angle. This can be accomplished by means of directly setting observation angle (when possible), or by means of reconstruction.

As for the magnitude response, previously measured OHC tuning curves have displayed sub-BF nonlinearity, which is larger when a multi-tone stimulus is applied.⁵ The OHC region also has been observed to be tuned less sharply than at the BM.^{5,6,18} These features appear across viewing angles, which is consistent with our finding that these characteristics are present in both the transverse and longitudinal components of motion (Fig. 7).

The characteristic similarities in phase observed in Fig. 10 provide evidence that the method is correctly reconstructing the transverse and longitudinal components of motion in the OHC-DC region. In particular, our original puzzle—that OHC-DC phase *leads* BM when measured at an angle with a substantial longitudinal component, and *lags* BM when measured at a transverse angle—is resolved by the reconstructions.

B. Physiological interpretations

The reconstructions presented emphasize the importance of accounting for, or at least reporting, the viewing angle used to collect displacement data. As in previous studies,¹⁰ we see that measurement angle can have a large impact on measured intra-OCC displacements, especially when considering the phase of motion.

Consistent with Cooper *et al.*, as well as Meenderink and Dong,²⁰ we see significant longitudinal motion that would appear opposite in polarity between measurements at viewing angles from apex-to-base and from base-to-apex.

As the OHCs are not significantly longitudinally slanted in the gerbil, this longitudinal component is not readily interpreted as a feature of electromotility.²¹ Instead, it may indicate the effects of fluid on these structures that is distinct from the BM. In addition, it may indicate the impact of other longitudinally tilted processes within the OCC on OHC-DC, for example, the phalangeal processes.^{15,21}

The phase lift at higher frequencies (near BF) seen in the reconstructions (Figs. 8 and 10), aligns the phase of OHC-DC transverse motion with that of BM motion. This can be interpreted as the OHC-DC transverse response having two modes—one that is due to moving along with the BM and one that is due to internal motions, such as elliptical fluid motion or electromotility. If the BM mode was much larger than the internal mode, the motion of the OHC-DC region would appear to be like BM motion. The appearance of the phase lift at relatively high SPL suggests a saturation and thus relative reduction of an active process. The lift appears here with a 70–80 dB Zwuis stimulus. A Zwuis stimulus with N individual tones set to a particular SPL is at an overall stimulus level approximately $10 \log N$ dB higher than that of a pure tone;^{5,22} for $N = 15$ this factor is 12 dB.

The reconstruction allows exploration of the elliptical transverse–longitudinal motion expected in the fluid ducts^{16,17} and believed to be present within the OCC.²⁰ In the reconstruction, we find that longitudinal and transverse components are related across frequency by a phase shift of approximately half a cycle. Geometrically, this would correspond to the motion within the OHC-DC region behaving as a *line*—a degenerate ellipse with an aspect ratio of 0—moving towards ST while moving towards the apex, and towards SV while moving towards the base. This is represented by the arrow in Fig. 5. Linear motion indicates that the motion at this particular location is not largely fluid-like. In scanning electron micrographs of the Deiters cells in the base of the mouse cochlea, the cells appear tightly packed,²³ resembling a sort of “wall” that would not allow the cells of the organ of Corti to behave simply as fluid. The longitudinally slanted phalangeal processes, radial tilt of the OHCs, and sturdy pillar cells^{15,23,24} are all part of a complex architecture, and cell groups are likely to move distinctly from one another in all three anatomical directions. OCT methods, such as the one presented in this study, can be used to study these properties.

The data used in this study was taken at relatively high sound pressure levels—70 and 80 dB SPL stimuli per tone. The SNR of the reconstructions is improved by an increase in angular difference and reconstruction at lower SPL would likely require a larger angular difference than we have achieved in the present work. Reconstructions at lower SPL would make a topic of future study.

V. EXTENSIONS OF THE METHOD

Here, we discuss two theoretical extensions of the method developed in Sec. II—one in which the accuracy of the method is improved by measuring from more than two longitudinal–transverse angles, and one in which the method

is extended to reconstruct all three anatomical components of motion. Similar to the strategy presented above, these techniques require only a single OCT beam and do not require any *a priori* knowledge of the measurement angles or precise locations of the structures being measured.

A. Overdetermined reconstruction

In the method presented above, we take measurements from two angles and solve a deterministic system of two linear equations in two variables. We noted the impact of noise in these measurements as it pertains to the condition number of the measurement matrix, which can be improved by increasing the angular difference between measurement angles. One could also improve the accuracy by employing the same experimental method, but measure structures at $M > 2$ angles. We call the measured displacements of a registered structure along these axes $\delta_1, \delta_2, \dots, \delta_M$ and write the respective measurement axes in terms of components $l_1, t_1, l_2, t_2, \dots, l_M, t_M$. At each registered location, one would now have a system of M equations in two variables—an overdetermined system. Mathematically, we can write the system as follows:

$$\begin{pmatrix} \delta_1 \\ \delta_2 \\ \vdots \\ \delta_M \end{pmatrix} = \begin{pmatrix} l_1 & t_1 \\ l_2 & t_2 \\ \vdots & \vdots \\ l_M & t_M \end{pmatrix} \begin{pmatrix} d_l \\ d_t \end{pmatrix}. \tag{20}$$

As a result of noise, this over-determined system will not have a solution—no value of the true motion \mathbf{d} can yield all M measured projections. Instead, we must find the most likely prediction of the true motion with noisy projection measurements.

The equation *actually* describing the projection at angle $m = 1, 2, \dots, M$ is

$$d_l l_m + d_t t_m + \mathcal{N}_m = \delta_m, \tag{21}$$

where \mathcal{N}_m is a realization of noise that is different in each measurement, and of course, unknown. Thereby, instead of trying to solve this equation, we try to minimize:

$$\mathcal{E} = \sum_{m=1}^M \|\delta_m - (d_l l_m + d_t t_m)\|^2. \tag{22}$$

The values of d_l and d_t that minimize \mathcal{E} are the least squares-optimal solution to this overdetermined problem.

In general, let \mathbf{x} and \mathbf{y} be vectors and A be a matrix. The least squares-optimal solution to an overdetermined linear system $\mathbf{y} = A\mathbf{x}$ is $\mathbf{x}_0 = A^\dagger \mathbf{y}$, where A^\dagger is the *Moore-Penrose pseudoinverse* of A . Most computational software packages include a routine to compute this pseudoinverse (for example, MATLAB’s `pinv`).

To employ this version of the method, one would take measurements at M angles along a large longitudinal stretch

as described in Sec. II. They would compute l_m and t_m for each orientation, and register points based on BM phase just as in the two-angle case. At each registered point, they will then reconstruct the true motion by

$$\mathbf{d} = \begin{pmatrix} l_1 & t_1 \\ l_2 & t_2 \\ \vdots & \vdots \\ l_M & t_M \end{pmatrix}^\dagger \begin{pmatrix} \delta_1 \\ \delta_2 \\ \vdots \\ \delta_M \end{pmatrix}. \tag{23}$$

Note that as the pseudoinverse of an invertible matrix is equal to the inverse of said matrix, this equation degenerates to Eq. (5) from the standard method in the $M = 2$ case.

B. Extension to three dimensions

Naturally, after 2-D reconstruction, one looks to the third spatial dimension—in this case, the radial dimension. To reconstruct 3-D motion requires motion measurements from three angles, and also requires at least one of the measurement axes to have a radial component.

First, let’s note the 3-D reconstruction formula as a simple generalization of the 2-D formula:

$$\begin{pmatrix} d_l \\ d_r \\ d_t \end{pmatrix} = \begin{pmatrix} l_1 & r_1 & t_1 \\ l_2 & r_2 & t_2 \\ l_3 & r_3 & t_3 \end{pmatrix}^{-1} \begin{pmatrix} \delta_1 \\ \delta_2 \\ \delta_3 \end{pmatrix}, \tag{24}$$

where δ_i are the measured displacements at angles $i = 1, 2, 3$, and $\hat{\mathbf{z}}_i = (l_i r_i t_i)^T$ is the measurement axis at angle i .

At each measurement angle, the longitudinal direction can still be computed in the same way, and longitudinally spaced measurements can still be taken along the cochlea just as before. As BM phase response does not vary across radial position within a single cross section, the registration method can be used just as before.

The only difference comes in determining the measurement matrix, which is now 3×3 . Our previously presented orientation program is well suited for the task.¹⁰ Given a volume scan at each orientation, this program can be used to approximate the anatomical components of the measurement axis. This would give $\hat{\mathbf{z}}_i$ for $i = 1, 2, 3$, and thereby allow for the complete 3-D reconstruction.

VI. CONCLUSIONS

We have presented a method for reconstructing transverse and longitudinal motion in the OCC and provided evidence of its utility by comparing data reconstructed at the OHC-DC location to previously measured transverse and longitudinal motion in the gerbil base. This method requires only a single OCT device, relying on reasonable assumptions regarding the vibration responses of the BM for registration. In the future, this method will be applied to other regions within the OCC to paint a more complete picture of micromechanical motion—in particular, it may help to

understand the impact of longitudinal fluid motion and longitudinally tilted processes in the OCC, and to probe the mechanical roles of supporting cells. It is also useful in isolating differences in measured responses due to viewing angle from those due to frequency location, species, or cochlear condition. The method can be applied without alteration to other frequency regions and species. Extensions of the method could be used to achieve a 3-D profile of intra-OCC motion, or to increase the fidelity of 2-D reconstructions.

¹J. A. Izatt and M. A. Choma, *Theory of Optical Coherence Tomography* (Springer Berlin Heidelberg, Berlin, Heidelberg, 2008), pp. 47–72.

²M. A. Choma, A. K. Ellerbee, C. Yang, T. L. Creazzo, and J. A. Izatt, “Spectral-domain phase microscopy,” *Opt. Lett.* **30**(10), 1162–1164 (2005).

³S. S. Gao, R. Wang, P. D. Raphael, Y. Moayedi, A. K. Groves, J. Zuo, B. E. Applegate, and J. S. Oghalai, “Vibration of the organ of Corti within the cochlear apex in mice,” *J. Neurophysiol.* **112**, 1192–1204 (2014).

⁴W. Dong, A. Xia, P. D. Raphael, S. Puria, B. E. Applegate, and J. S. Oghalai, “Organ of Corti vibration within the intact gerbil cochlea measured by volumetric optical coherence tomography and vibrometry,” *J. Neurophysiol.* **120**, 2847–2857 (2018).

⁵E. Fallah, C. E. Strimbu, and E. S. Olson, “Nonlinearity and amplification in cochlear responses to single and multi-tone stimuli,” *Hear. Res.* **377**, 271–281 (2019).

⁶C. E. Strimbu, Y. Wang, and E. S. Olson, “Manipulation of the endocochlear potential reveals two distinct types of cochlear nonlinearity,” *Biophys. J.* **119**(10), 2087–2101 (2020).

⁷F. Chen, D. Zha, A. Fridberger, J. Zheng, N. Choudhury, S. L. Jacques, R. K. Wang, X. Shi, and A. L. Nuttall, “A differentially amplified motion in the ear for near-threshold sound detection,” *Nat. Neurosci.* **14**(6), 770–774 (2011).

⁸H. Y. Lee, P. D. Raphael, A. Xia, J. Kim, N. Grillet, B. E. Applegate, A. K. E. Bowden, and J. S. Oghalai, “Two-dimensional cochlear micromechanics measured *in vivo* demonstrate radial tuning within the mouse organ of Corti,” *J. Neurosci.* **36**(31), 8160–8173 (2016).

⁹N. P. Cooper, A. Vavakou, and M. Van Der Heijden, “Vibration hotspots reveal longitudinal funneling of sound-evoked motion in the mammalian cochlea,” *Nat. Commun.* **9**(1), 3054–3064 (2018).

¹⁰B. L. Frost, C. E. Strimbu, and E. S. Olson, “Using volumetric optical coherence tomography to achieve spatially resolved organ of Corti vibration measurements,” *J. Acoust. Soc. Am.* **151**, 1115–1125 (2022).

¹¹N. H. Cho and S. Puria, “Motion of the cochlear reticular lamina varies radially across outer-hair-cell rows,” bioRxiv (2022), <https://www.biorxiv.org/content/early/2022/03/04/2022.03.01.482580>.

¹²W. He, G. Burwood, E. V. Porsov, A. Fridberger, A. L. Nuttall, and T. Ren, “The reticular lamina and basilar membrane vibrations in the transverse direction in the basal turn of the living gerbil cochlea,” *Sci. Rep.* **12**(1), 19810–19820 (2022).

¹³W. Kim, D. Liu, S. Kim, K. Ratnayake, F. Macias-Escriva, S. Mattison, J. S. Oghalai, and B. E. Applegate, “Vector of motion measurements in the living cochlea using a 3d oct vibrometry system,” *Biomed. Opt. Express* **13**, 2542–2553 (2022).

¹⁴E. Fallah, C. E. Strimbu, and E. S. Olson, “Nonlinearity of intracochlear motion and local cochlear microphonic: Comparison between guinea pig and gerbil,” *Hear. Res.* **405**, 108234–108246 (2021).

¹⁵P. Dallos, A. N. Popper, R. R. Fay, and N. B. Slepecky, *Structure of the Mammalian Cochlea* (Springer, New York), pp. 44–129.

¹⁶J. Lighthill, *Waves in Fluids* (Cambridge University Press, Cambridge, UK, 1978).

¹⁷J. Lighthill, “Energy flow in the cochlea,” *J. Fluid Mech.* **106**, 149–213 (1981)..

¹⁸C. E. Strimbu and E. S. Olson, “Salicylate-induced changes in organ of Corti vibrations,” *Hear. Res.* **423**, 108389–108400 (2022).

¹⁹D. D. Greenwood, “A cochlear frequency-position function for several species—29 years later,” *J. Acoust. Soc. Am.* **87**, 2592–2605 (1990).

²⁰S. Meenderink and W. Dong, “Organ of Corti vibrations are dominated by longitudinal motion *in vivo*,” *Commun. Biol.* **5**, 1285–1289 (2022).

²¹Y.-J. Yoon, C. R. Steele, and S. Puria, “Feed-forward and feed-backward amplification model from cochlear cytoarchitecture: An interspecies comparison,” *Biophys. J.* **100**, 1–10 (2011).

²²C. P. Versteegh and M. van der Heijden, “Basilar membrane responses to tones and tone complexes: Nonlinear effects of stimulus intensity,” *J. Assoc. Res. Otolaryngol.* **13**, 785–798 (2012).

²³A. Parsa, P. Webster, and F. Kalinec, “Deiters cells tread a narrow path—The Deiters cells-basilar membrane junction,” *Hear. Res.* **290**(1-2), 13–20 (2012).

²⁴W. Zhou, T. Jabeen, S. Sabha, J. Becker, and J.-H. Nam, “Deiters cells act as mechanical equalizers for outer hair cells,” *J. Neurosci.* **42**(44), 8361–8372 (2022).